

Energy dependence of the optical potential of weakly and tightly bound nuclei as projectiles on a medium-mass target

J. M. Figueira,^{1,2,*} J. O. Fernández Niello,^{1,2,3} A. Arazi,^{1,2} O. A. Capurro,¹ P. Carnelli,^{1,2} L. Fimiani,¹ G. V. Martí,¹ D. Martínez Heimann,^{1,2} A. E. Negri,^{1,2} A. J. Pacheco,^{1,2} J. Lubian,⁴ D. S. Monteiro,⁴ and P. R. S. Gomes⁴

¹Laboratorio Tandar, Comisión Nacional de Energía Atómica, B1650KNA San Martín, Buenos Aires, Argentina

²Consejo Nacional de Investigaciones Científicas y Técnicas, C1033AAJ Ciudad de Buenos Aires, Argentina

³Escuela de Ciencia y Tecnología, Universidad de San Martín, B1650BWA San Martín, Buenos Aires, Argentina

⁴Instituto de Física, Universidade Federal Fluminense, Gragoatá, Niterói, R. J., 24210-340, Brazil

(Received 16 October 2009; published 25 February 2010)

Angular distributions for the elastic scattering of the weakly bound ${}^6,7\text{Li} + {}^{144}\text{Sm}$ systems were measured with high accuracy at bombarding energies from 85% up to 170% of the Coulomb barrier. An optical model analysis was performed, and the relevant parameters of the real and imaginary parts of the optical potential were extracted. The results are compared with those previously published for the tightly bound ${}^{12}\text{C} + {}^{144}\text{Sm}$ and ${}^{16}\text{O} + {}^{144}\text{Sm}$ systems. The usual threshold anomaly observed in the behavior of the potential of tightly bound systems was not observed for either weakly bound system. This absence is attributed to the repulsion due to breakup coupling which cancels the attraction arising from couplings with bound channels.

DOI: [10.1103/PhysRevC.81.024613](https://doi.org/10.1103/PhysRevC.81.024613)

PACS number(s): 25.70.Bc, 24.10.Ht, 25.70.Mn

I. INTRODUCTION

The strong influence that the breakup process may exert on other reaction channels in systems that involve weakly bound nuclei has become a subject of considerable interest in recent years [1–20]. Breakup reactions can be studied experimentally in a variety of ways. On the one hand, the detection of the breakup fragments either in inclusive or exclusive experiments can directly furnish the cross sections for this process as a function of the bombarding energy and its behavior in the vicinity of the Coulomb barrier. In particular, exclusive measurements through the coincident detection of both emitted fragments can be especially sensitive for the identification and characterization of breakup mechanisms, although these measurements are often associated with lengthy experiments [20–30]. On the other hand, a complementary approach to the study of the effect of breakup on other reaction processes is the systematic analysis of the behavior of the optical potentials used to describe elastic scattering.

In systems formed with tightly bound nuclei, the elastic scattering close to the Coulomb barrier as described by the optical model shows a rapid variation of both the real and imaginary parts of the potential as a function of the bombarding energy. The real part of the potential exhibits a bump at values close to the Coulomb barrier and the imaginary part decreases from a constant value at above-barrier energies down to almost zero at energies below the barrier. This behavior of both parts of the potential close to the Coulomb barrier, known as the threshold anomaly (TA), is consistent with a dispersion relation that correlates the energy dependence of the real and imaginary parts of the optical potential [31–34] due to causality [34–36], which imposes the condition that no scattered wave emerges before the incident wave reaches the target.

If one of the reaction partners is a weakly bound nucleus, the dynamics of the collision will change, modifying the cross sections in the elastic channel. It is possible that the breakup channel does not close as a function of decreasing energy as fast as other channels in the vicinity of the Coulomb barrier and, hence, the behavior of the optical potential under such circumstances can be different from the tightly bound system. In some works [37–41] an increase of the imaginary potential at lower energies (and, due to the dispersion relation, a decrease of the real part of the potential) has been observed which is known as breakup threshold anomaly.

The effect of small binding energies on the elastic scattering channel can be investigated using beams of weakly bound stable nuclei, like ${}^6\text{Li}$ and ${}^7\text{Li}$. These nuclei break up into $\alpha + d$ and $\alpha + t$ and have the low threshold breakup energies of 1.47 and 2.47 MeV, respectively. Thus, the probability for breakup is significant.

In this article we present 22 angular distributions of original and high-precision experimental elastic-scattering cross sections of weakly bound ${}^6\text{Li}$ and ${}^7\text{Li}$ nuclei from the neutron magic ${}^{144}\text{Sm}$ target taken in a wide range of bombarding energies (Sec. II). Performing a χ^2 analysis within the framework of the optical model, we found phenomenological energy-dependent optical potentials that describe the experimental elastic angular distributions (Sec. III). We carried out a dispersion relation calculation to see whether it was satisfied, and we obtained a qualitative agreement between the theory and the data (Sec. III). We observed, for both weakly bound ${}^6,7\text{Li} + {}^{144}\text{Sm}$ systems, that the energy dependence of the potentials do not show the usual threshold anomaly which has always been seen in tightly bound systems (Sec. IV). This work is part of a more extended research project aiming to explore the influence of the breakup of those projectiles on targets having different masses and deformations [16–19,38–56].

* figueira@tandar.cnea.gov.ar

II. EXPERIMENTAL SETUP

Angular distributions of elastic scattering differential cross sections for the ${}^7\text{Li}$ and ${}^6\text{Li} + {}^{144}\text{Sm}$ systems were measured using beams delivered by the 20 UD tandem accelerator at the TANDAR Laboratory. Typical beam currents were of the order of 20 pA. The Coulomb barriers in the laboratory frame are, following the prescription given in Ref. [57], $V_b^{\text{lab}} = 24.3$ MeV and 24.5 MeV for ${}^7\text{Li}$ and ${}^6\text{Li} + {}^{144}\text{Sm}$, respectively. The angular distributions were obtained at eleven different bombarding energies for each projectile in the ranges 21.6–40.8 MeV for ${}^7\text{Li}$ and 21.0–42.3 MeV for ${}^6\text{Li}$ (approximately 85% below to 170% above the nominal Coulomb barrier). The beams impinged on a $120\text{-}\mu\text{g}/\text{cm}^2$ -thick ${}^{144}\text{Sm}$ target. The material was isotopically enriched to 88%, and it was evaporated onto a $20\text{-}\mu\text{g}/\text{cm}^2$ carbon backing. The energy spread of the beam was around 0.5%, mainly due to the 10-mm aperture of the analyzing magnet slits. The effect of energy straggling within the target accounts for an additional energy spread of at most 0.2%.

The detection system consisted of an array containing eight silicon surface-barrier detectors placed in a 76-cm-diameter scattering chamber. The angular separation between the collimators of two adjacent detectors was 5° and the angular resolution of each detector was better than 0.5° . The elastic-scattering angular distributions were taken in steps of 2.5° or 5.0° depending on the beam energy and angular range. The energy resolution of the detectors ranged from 0.5% to 1.0%.

Absolute cross sections were obtained from the number of counts in the elastic peaks, normalized by the counts simultaneously registered on a monitor detector placed at a fixed angle of 12.9° . At this angular position the validity of the Rutherford cross-section formula is ensured. The solid-angle ratios between each detector of the array and the monitor, which are necessary for the determination of absolute cross sections, were determined by measuring the elastic scattering of ${}^7\text{Li}$ and ${}^{16}\text{O}$ from a $200\text{-}\mu\text{g}/\text{cm}^2$ -thick ${}^{197}\text{Au}$ target at bombarding energies 60% below the Coulomb barrier (where the Rutherford cross section holds at all angles).

The statistical uncertainty of the cross sections ranges from 2 to 20%, the latter corresponding to the highest energies and backward angles. The contribution due to the target contaminants was estimated to be about 2% from their known abundances. The experimental angular distributions of the elastic scattering cross sections normalized to the Rutherford cross section are shown in Figs. 1 and 2 for ${}^7\text{Li} + {}^{144}\text{Sm}$ and ${}^6\text{Li} + {}^{144}\text{Sm}$, respectively.

III. OPTICAL MODEL ANALYSIS AND DISPERSION RELATION CALCULATIONS

The elastic-scattering differential cross sections measured in this work were analyzed using a phenomenological potential given by

$$U(r) = V_{\text{coul}}(r) - Vf(r, R_V, a_V) - i W_V f(r, R_{WV}, a_{WV}) - i W_S g(r, R_{WS}, a_{WS}). \quad (1)$$

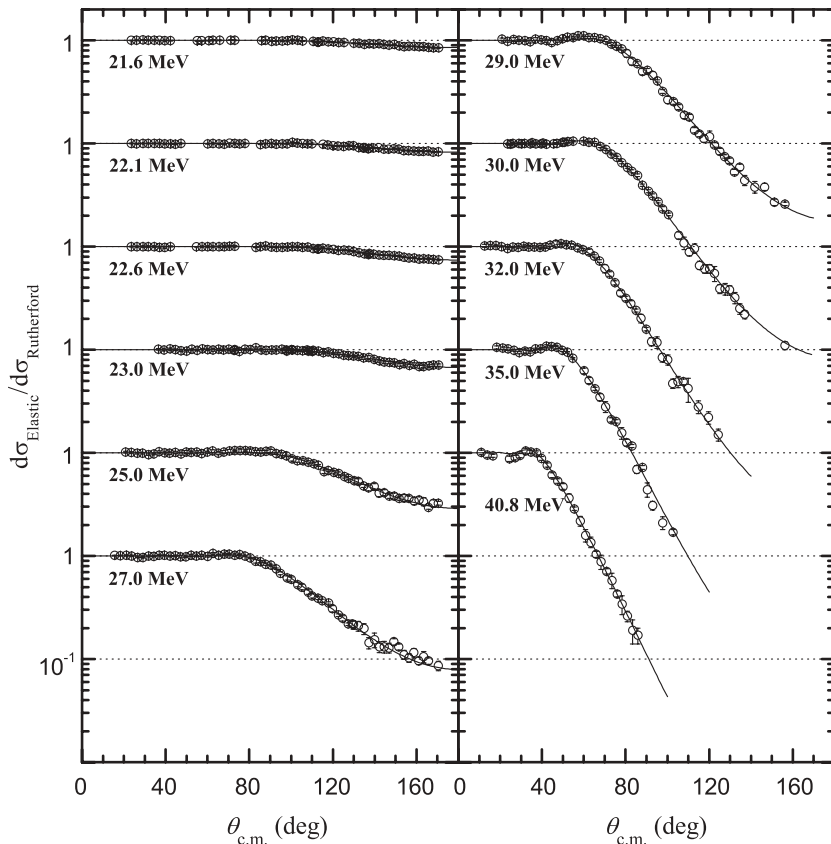


FIG. 1. Experimental elastic-scattering cross sections normalized to the Rutherford cross sections for the ${}^7\text{Li} + {}^{144}\text{Sm}$ system (open circles) and their best fits from optical model calculations (solid curves). Energies are given in the laboratory frame.

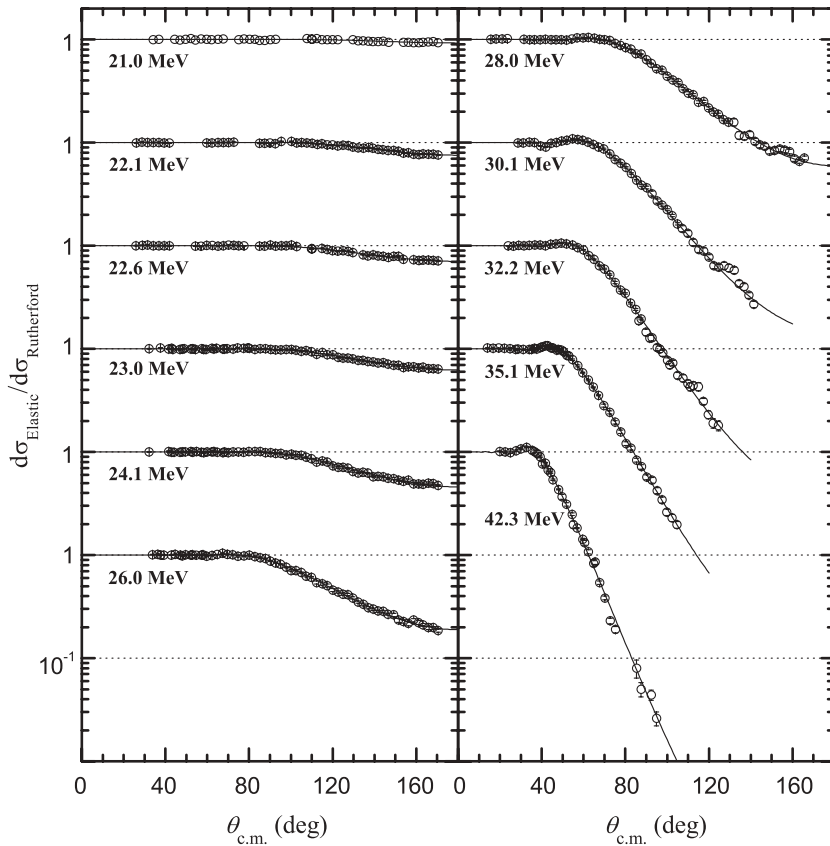


FIG. 2. Experimental elastic scattering cross sections normalized to the Rutherford cross sections for the ${}^6\text{Li} + {}^{144}\text{Sm}$ system (open circles) and their best fits from optical model calculations (solid curves). Energies are given in the laboratory frame.

In the first term of Eq. (1), V_{coul} is the Coulomb potential of a uniformly charged sphere of radius $R_C = 1.2(A_p^{1/3} + A_t^{1/3})$ fm. In the second and third term of Eq. (1), f is the Woods-Saxon form factor given by

$$f(r, R_i, a_i) = \left[1 + \exp\left(\frac{r - R_i}{a_i}\right) \right]^{-1},$$

where R_i is the radius and a_i is the diffuseness. The radius R_i is usually expressed in terms of the reduced radius r_i , defined as $R_i = r_i(A_p^{1/3} + A_t^{1/3})$, A_p and A_t being the projectile and target mass numbers, respectively. In the last term of Eq. (1), g is the derivative of the Woods-Saxon form factor given by $g(r, R_i, a_i) = 4a_i df/dr(r, R_i, a_i)$ which peaks at the surface of the nucleus. The last term of the optical potential U is therefore known as the surface imaginary potential, and W_S represents its depth. Analogously, the imaginary term of U which contains the form factor f , owed to its geometry is called the volume imaginary potential and W_V represents its depth. The real part of the potential U which contains the form factor f has a depth given by V .

The surface imaginary potential is introduced to take into account the absorption from peripheral processes (inelastic scattering, particle transfers, and breakup) since these mainly occur at distances close to R_C , while the imaginary volume potential is introduced to take into account the absorption from fusion, as this process occurs predominantly at distances which are shorter than R_C .

To summarize, within this phenomenological framework there are nine parameters available to adjust: the three depths

V , W_V , and W_S , the three reduced radii r_V , r_{W_V} , and r_{W_S} , and the three diffusenesses a_V , a_{W_V} , and a_{W_S} . Due to this large number of parameters the process of adjusting the theory to experimental data is not necessarily free of ambiguities; that is to say, that different families of parameters may describe the data equally well, including some with parameter values which do not make physical sense.

In this work, all optical model calculations were carried out using the code PTOLEMY [58,59]. In order to obtain the optical potential parameters, we performed a simultaneous best fit procedure for the angular distributions of the ${}^7\text{Li} + {}^{144}\text{Sm}$ system's three higher energies, with the constraints $r_{W_V} < r_V = r_{W_S}$ and $a_V = a_{W_S}$. As the result of this simultaneous analysis we obtained the following optical-potential parameter values: the depths $V = 14.0$ MeV, $W_S = 4.13$ MeV, and $W_V = 6.30$ MeV, the reduced radii $r_V = r_{W_S} = 1.25$ fm and $r_{W_V} = 1.05$ fm, and the diffusenesses $a_V = a_{W_S} = 0.70$ fm and $a_{W_V} = 0.714$ fm. Later, we performed independent fits to each elastic-scattering angular distribution at each different energy, keeping as fixed parameters those corresponding to the internal volume imaginary potential and those to the radii and diffuseness of the real and surface imaginary potentials. The depths V and W_S were left as free parameters allowing an energy dependence in the optical potential. In that way, correlated ambiguities in the parameter values were confined to only two variable parameters [33] and due to the allowed energy dependence of the potentials the fits to the angular distributions were improved. The results of V and W_S obtained for each energy are presented in Table I and the corresponding fits are shown in Figs. 1 and 2. The small oscillations present

TABLE I. Summary of the optical potentials at different energies for ${}^7\text{Li} + {}^{144}\text{Sm}$ and ${}^6\text{Li} + {}^{144}\text{Sm}$ systems obtained from the optical model fit procedure performed on the elastic-scattering angular distributions. For both systems, the internal volume imaginary potential parameters were $W_V = 6.3$ MeV, $r_{WV} = 1.05$ fm, and $a_{WV} = 0.714$ fm, and the reduced radii and diffusenesses of the real and surface imaginary parts were $r_V = r_{WS} = 1.25$ fm and $a_V = a_{WS} = 0.70$ fm. $V(\bar{R}_S)$ and $W(\bar{R}_S)$ are, respectively, the real and total imaginary potentials ($W = W_V + W_S$) evaluated at the sensitivity radius \bar{R}_S . For the ${}^7\text{Li} + {}^{144}\text{Sm}$ system $\bar{R}_S = 11.63$ fm and for the ${}^6\text{Li} + {}^{144}\text{Sm}$ system $\bar{R}_S = 11.59$ fm. The χ^2/point of the fits are given at each energy. The overall χ^2/point for the ${}^7\text{Li} + {}^{144}\text{Sm}$ and ${}^6\text{Li} + {}^{144}\text{Sm}$ systems were 1.296 and 2.372, respectively.

${}^7\text{Li} + {}^{144}\text{Sm}$						${}^6\text{Li} + {}^{144}\text{Sm}$					
$E_{c.m.}$	V	W_S	$V(\bar{R}_S)$	$W(\bar{R}_S)$	χ^2/point	$E_{c.m.}$	V	W_S	$V(\bar{R}_S)$	$W(\bar{R}_S)$	χ^2/point
20.6	21.3	4.94	0.45	0.42	1.21	20.2	33.8	1.90	0.64	0.16	1.20
21.0	21.4	3.42	0.45	0.30	1.44	21.2	38.0	4.05	0.72	0.32	2.21
21.5	21.0	3.78	0.44	0.33	0.87	21.6	25.0	5.64	0.47	0.44	2.24
21.9	21.8	3.27	0.46	0.29	0.59	22.1	18.7	6.78	0.35	0.52	1.35
23.8	17.7	3.58	0.37	0.31	1.17	23.1	16.9	6.03	0.32	0.46	1.78
25.7	15.6	4.06	0.33	0.35	1.62	25.0	14.7	5.63	0.28	0.44	1.45
27.7	15.2	3.77	0.32	0.33	2.09	26.9	13.9	5.60	0.26	0.43	1.66
28.6	14.9	3.45	0.31	0.30	0.92	28.9	15.0	4.94	0.28	0.38	6.65
30.5	15.2	4.04	0.32	0.35	1.34	30.9	15.9	4.56	0.30	0.36	2.02
33.4	12.8	4.01	0.27	0.35	2.52	33.7	15.6	5.32	0.29	0.41	2.87
38.9	8.58	7.18	0.18	0.61	0.88	40.6	14.4	3.92	0.27	0.31	4.25

in the angular distributions at larger angles and higher energies could not be satisfactorily adjusted even with drastic variations of the imaginary potential depth and geometrical parameters.

Ambiguities coming from the multiparameter fit procedure can be absolutely removed if the potentials are evaluated at the sensitivity radius R_S [33] at each energy. R_S is defined as the value of the radial coordinate where different potentials with comparable goodness of fit (i.e., with similar χ^2) intersect each other (i.e., take the same value) (see Refs. [17,60–63]). Heavy-ion elastic scattering is most sensitive in the nuclear-surface region and hence it primarily determines, at each energy, the potential values in the vicinity of the sensitivity radius [33]. This sensitivity radius has a slight energy dependence [33]. For the real part of the potential, we calculated the corresponding value of R_S (at each bombarding energy) in the following way: with $a_{V_{\min}}$ and χ^2_{\min} being the diffuseness parameter of the potential and the goodness of the best fit obtained in the χ^2 -minimization procedure, we performed four new fits of the data keeping the diffuseness as fixed parameters but with slight modifications from $a_{V_{\min}}$ (steps of 0.02 fm) and keeping as free parameters the radius parameter r_V and the potential depth V . In this way, we found a family of five optical potentials with roughly the same χ^2 , and the sensitivity radius from the radial position where all the potentials in the family intersect each other (for a graphical example see Fig. 3 of Ref. [17]). In an analogous way, following this procedure we found the sensitivity radius of the surface imaginary potential at each bombarding energy. The obtained sensitivity radii at the different energies for the real part (R_{S_V}) and for the surface imaginary part ($R_{S_{W_S}}$) are shown in Fig. 3(a) and Fig. 3(b) for the ${}^7\text{Li} + {}^{144}\text{Sm}$ and the ${}^6\text{Li} + {}^{144}\text{Sm}$ systems, respectively. For both systems, both R_{S_V} and $R_{S_{W_S}}$ show a slight energy dependence, becoming smaller as the bombarding energy increases. It can be seen that the dependence is stronger at sub-barrier energies and vanishes as the energy increases toward the Coulomb barrier, and the sensitivity radii remains

almost constant at energies above ~ 28 MeV. The mean values of the sensitivity radii of each system are $\bar{R}_S = 11.63$ fm and $\bar{R}_S = 11.59$ fm for ${}^7\text{Li} + {}^{144}\text{Sm}$ and ${}^6\text{Li} + {}^{144}\text{Sm}$, respectively. The uncertainty intervals in the potential depths were deduced from the change of the total χ^2 in one unity and hence, they correspond to a confidence level of 68.3%.

In what follows, we analyze whether the obtained energy-dependent potentials satisfy the dispersion relation, which connects the real and imaginary parts through the expression

$$V(E, r) = V_0 + \frac{1}{\pi} \mathbf{P} \int_{-\infty}^{+\infty} \frac{W(E', r)}{E' - E} dE',$$

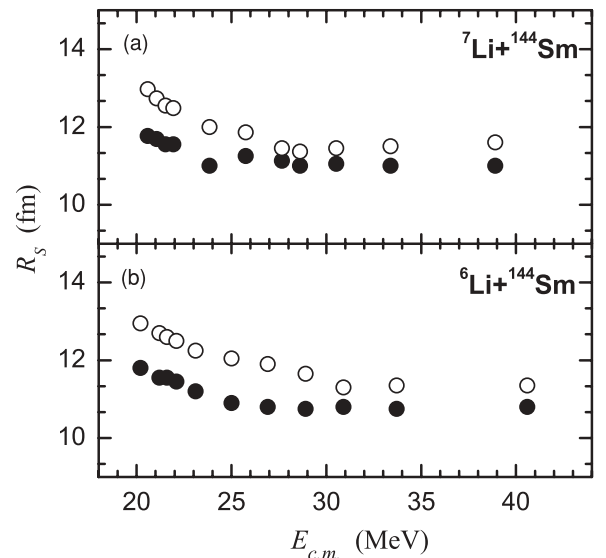


FIG. 3. Sensitivity radii R_{S_V} (full circles) and $R_{S_{W_S}}$ (open circles) for (a) ${}^7\text{Li} + {}^{144}\text{Sm}$ and (b) ${}^6\text{Li} + {}^{144}\text{Sm}$. They remain almost constant at energies above ~ 28 MeV and increase slightly as the energy goes down from close to the top of Coulomb barrier.

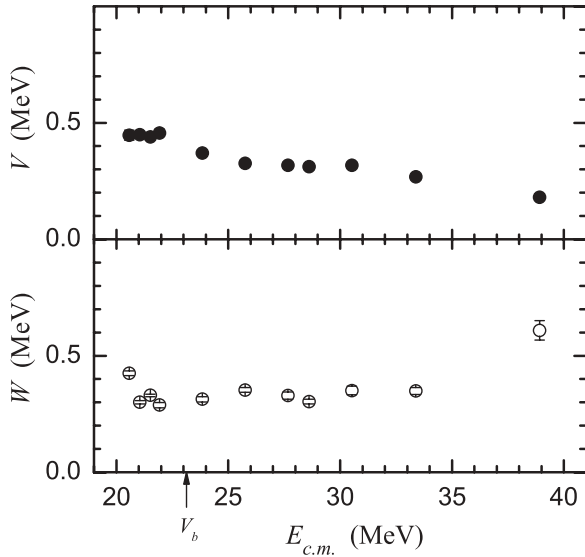


FIG. 4. Energy dependence of the real and imaginary parts of the optical potential obtained for ${}^7\text{Li} + {}^{144}\text{Sm}$ system at an average radius $\bar{R}_S = 11.63$ fm. The energy V_b of the Coulomb barrier is indicated.

where \mathbf{P} denotes the principal value, V_0 is a constant offset, and W is the total imaginary potential [i.e., $W(E, r) = W_V(E, r) + W_S(E, r)$]. Because the sensitivity radius is not strictly constant at different energies (as illustrated in Fig. 3), it is customary to evaluate the real and imaginary parts of the empirical optical potential at a fixed radius close to the sensitivity one [32,33,64,65]; we chose the mean value of sensitivity radius \bar{R}_S .

The empirical real and imaginary parts of the optical potential at the mean sensitivity radius for the ${}^7\text{Li} + {}^{144}\text{Sm}$ and the ${}^6\text{Li} + {}^{144}\text{Sm}$ systems are shown in Figs. 4 and 5, respectively. For the dispersion relation calculations shown in Fig. 5 (corresponding to the ${}^6\text{Li}$ case) we used the model proposed in Ref. [34], where $W(E)$ is represented schematically by a series of linear segments but has the advantage of giving an analytic form of the dispersion relation. Each line segment associated with an increment $W_{ij} = W(E_i) - W(E_j)$ yields the contribution

$$\Delta V_{ij}(E) = V_{ij}(E) - V_0 = (W_{ij}/\pi)(\varepsilon_i \ln |\varepsilon_i| - \varepsilon_j \ln |\varepsilon_j|),$$

where $\varepsilon_i = (E - E_i)/\Delta_{ij}$, $\varepsilon_j = (E - E_j)/\Delta_{ij}$ and $\Delta_{ij} = (E_j - E_i) > 0$. Two different fits were made in order to demonstrate the sensitivity of the calculated $V(E)$ to changes in $W(E)$. It can be seen that there is a qualitative agreement between the empirical and calculated values of the real potential $V(E)$, showing that the dispersion relation is satisfied.

IV. DISCUSSION

For the ${}^7\text{Li} + {}^{144}\text{Sm}$ system (see Fig. 4), the behavior of the real and imaginary parts of the energy-dependent optical potential does not correspond to the usual threshold anomaly. Instead of vanishing near the Coulomb barrier (as occurs in systems where the threshold anomaly is present), the imaginary potential almost does not vary as a function of the energy except for the lowest measured energy, which lies

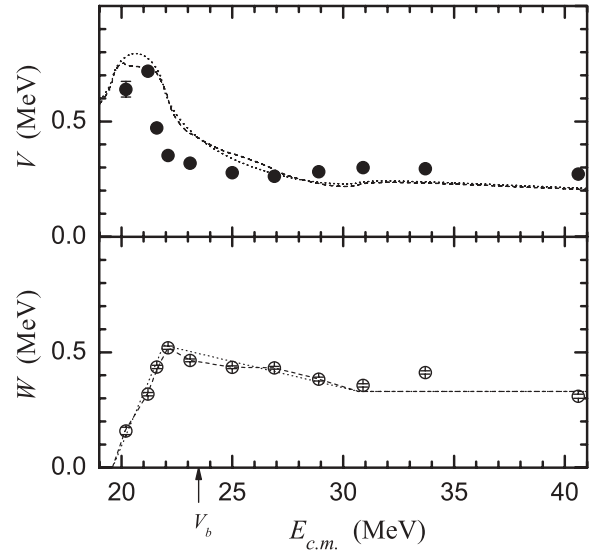


FIG. 5. Energy dependence of the real and imaginary parts of the optical potential obtained for ${}^6\text{Li} + {}^{144}\text{Sm}$ system at an average radius $\bar{R}_S = 11.59$ fm. The energy V_b of the Coulomb barrier is indicated. The dotted and dashed lines in the bottom frame are two different schematic linear-segment fits of the imaginary potential $W(E)$ that lead, by means of the dispersion relation, to the lines representing the real potential $V(E)$ in the top frame.

slightly above the rest. This is an important result which means that for that system there are one or more absorptive channels still open at energies below the barrier. Even though the real part of the energy-dependent optical potential smoothly increases as the energy decreases, this smooth increase could be considered as consistent (through the dispersion relation) with a constant imaginary part as has been obtained.

In the case of ${}^6\text{Li} + {}^{144}\text{Sm}$ system (see Fig. 5), the imaginary potential is still large at the Coulomb barrier and even slightly below, and again, as in the ${}^7\text{Li}$ case, it means that the absorption is still significant for that energy regime and that the usual threshold anomaly is not present. In Fig. 5 we have included two different schematic linear segment fits of the imaginary potential leading, through the dispersion relation, to the corresponding schematic lines of the real potential at the top frame.

However, there is a remarkable difference between both weakly bound systems: The imaginary part of the optical potential for the ${}^6\text{Li}$ projectile, instead of being almost constant as a function of energy (as it is for the ${}^7\text{Li}$), slightly increases as the energy decreases from 31 to 22 MeV and finally it quickly drops to zero below this energy.

To emphasize the differences of the weakly bound systems relative to the tightly bound systems, we show in Fig. 6 a comparison between the results obtained for the ${}^{6,7}\text{Li} + {}^{144}\text{Sm}$ weakly bound systems and those obtained in Refs. [61,62] for the tightly bound projectiles ${}^{12}\text{C}$ and ${}^{16}\text{O}$ on a ${}^{144}\text{Sm}$ target. In order to make a consistent comparison we used the same approaches to obtain the optical potentials as was used by Abriola *et al.* Because we only want to point out the main differences between the potential strengths at the Coulomb barrier, they are shown as a function of the energy to Coulomb

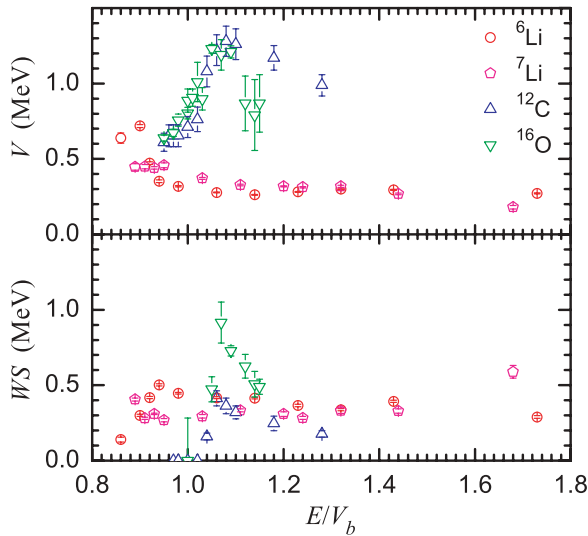


FIG. 6. (Color online) Real and imaginary parts of the optical potentials for the weakly bound systems ${}^6\text{Li} + {}^{144}\text{Sm}$ and ${}^7\text{Li} + {}^{144}\text{Sm}$ obtained in this work and those for the tightly bound systems ${}^{12}\text{C} + {}^{144}\text{Sm}$ and ${}^{16}\text{O} + {}^{144}\text{Sm}$ taken from Refs. [61,62]. For comparison, the potentials of each system are shown as a function of the ratio of the energy to their corresponding Coulomb barriers V_b .

barrier ratio (E/V_b). In the same way as for the ${}^{6,7}\text{Li} + {}^{144}\text{Sm}$ systems, the Coulomb barrier of the ${}^{12}\text{C}$ and ${}^{16}\text{O} + {}^{144}\text{Sm}$ systems were calculated to be $V_b^{\text{lab}} = 49.2$ MeV and 66.1 MeV, respectively, following Ref. [57]. For the tightly bound ${}^{12}\text{C}$ and ${}^{16}\text{O}$ projectiles, the optical potentials are observed to have a strong variation at energies slightly above the Coulomb barrier in accordance with the threshold anomaly. The real parts of the optical potentials exhibit a bump centered at E/V_b approximately 1.07, and from this value of E/V_b the imaginary parts drop quickly to zero as the energy decreases toward the Coulomb barrier. The behavior of the imaginary and real parts satisfy the dispersion relation and was interpreted as evidence of the presence of the threshold anomaly for both tightly bound systems [61,62]. On the other hand, the ${}^6\text{Li}$ and ${}^7\text{Li}$ systems do not show the same behavior at the Coulomb barrier. As stated above, for ${}^7\text{Li} + {}^{144}\text{Sm}$ the imaginary part of the potential is almost constant for all the measured energy points, i.e., until E/V_b approximately 0.90. For ${}^6\text{Li} + {}^{144}\text{Sm}$ there is an increase in the strength of the imaginary part as E/V_b decreases from near 1.25 to approximately 0.95, and from that value it drops to zero vanishing at E/V_b approximately 0.82. The noticeable difference between ${}^6\text{Li}$ and both tightly bound projectiles is that in the latter case the absorptive channels close at energies above the Coulomb barrier while in the former case the absorptive channels remain open even at sub-barrier energies, as can be seen from the shift in energy at which W_S drops to zero. At higher energies, although all these systems differ in the absolute strengths, they exhibit a similar pattern as a function of the energy.

The behavior of the imaginary part of the optical potential just described for ${}^6\text{Li} + {}^{144}\text{Sm}$ (i.e., an increase of the imaginary strength as a function of decreasing energy even at energies slightly below the Coulomb barrier) has also

been observed in other reactions induced by weakly bound projectiles such as ${}^9\text{Be} + {}^{64}\text{Zn}$ [38], ${}^9\text{Be} + {}^{209}\text{Bi}$ [44], ${}^6\text{Li} + {}^{208}\text{Pb}$ [39], ${}^6\text{Li} + {}^{27}\text{Al}$ [40], ${}^6\text{Li} + {}^{58}\text{Ni}$ and ${}^6\text{Li} + {}^{64}\text{Ni}$ [6], and ${}^6\text{Li} + {}^{90}\text{Zr}$ [41]. In recent works [38,39] it has been speculated that this energy dependence could be a fingerprint of the influence exerted by the breakup channel which is expected to be dominant in these systems even at energies below the barrier, and the denomination breakup threshold anomaly was coined. From Fig. 6 it should be noted however that the increase of the imaginary strength as a function of decreasing energy down to the Coulomb barrier is also present in the reactions induced by the tightly bound projectiles ${}^{12}\text{C}$ and ${}^{16}\text{O}$ on the same ${}^{144}\text{Sm}$ target, but with the important difference that the increasing regions are completely positioned at energies above the top of the Coulomb barrier while for the weakly bound projectiles presenting the so-called breakup threshold anomaly the increasing regions extend until above the Coulomb barrier because the breakup channel remains open.

We believe that the present results adequately placed in the framework of previous measurements call for further investigation of the influence played by the breakup channel through the measurement of weakly bound and tightly bound projectiles on different targets, especially at energies well below the Coulomb barrier.

V. SUMMARY AND CONCLUSIONS

In this work we present an exhaustive measurement of elastic angular distributions for the ${}^{6,7}\text{Li} + {}^{144}\text{Sm}$ systems at 11 bombarding energies for each system covering a broad energy range from 0.85 to almost 1.7 times the Coulomb barrier. They have been measured with sufficient accuracy to extract reliable values for the optical potentials in order to investigate how the projectile breakup channel influences their behaviors. The novel results obtained for the ${}^{6,7}\text{Li} + {}^{144}\text{Sm}$ systems show that the imaginary part of the optical potentials do not vanish at the Coulomb barrier and, therefore, that there is an absence of the usual threshold anomaly observed in tightly bound systems for which the imaginary part of the optical potential vanishes at the Coulomb barrier.

We have stated that the two systems formed with the weakly bound ${}^6\text{Li}$ and ${}^7\text{Li}$ projectiles behave differently: While the imaginary part of the optical potential for the ${}^6\text{Li} + {}^{144}\text{Sm}$ falls to zero as the energy decreases below the Coulomb barrier, this is not observed for ${}^7\text{Li}$. We have also found an energy dependence of the real and imaginary potentials for the ${}^6\text{Li} + {}^{144}\text{Sm}$ system that resembles the one for the systems formed with the tightly bound ${}^{12}\text{C}$ and ${}^{16}\text{O}$ projectiles on the same ${}^{144}\text{Sm}$ target, but with the important difference that in the former case the imaginary part still survives at energies below the Coulomb barrier.

We attribute the fact that the imaginary part of the optical potentials for the ${}^{6,7}\text{Li} + {}^{144}\text{Sm}$ systems do not vanish at the Coulomb barrier (as does occur for tightly bound systems) as an indication that the repulsion due to breakup coupling cancels the attraction arising from couplings with bound channels, as has already been interpreted and pointed out in Refs. [13,17,39,41,51].

ACKNOWLEDGMENTS

We acknowledge help from G. Abelof, D. Barmak during various stages of the experiment and A. E. Woodard for her

useful suggestions and careful reading of this manuscript. This work was partially supported by the CNPq, FAPERJ, and Proslu.

- [1] D. J. Hinde, M. Dasgupta, B. R. Fulton, C. R. Morton, R. J. Wooliscroft, A. C. Berriman, and K. Hagino, *Phys. Rev. Lett.* **89**, 272701 (2002).
- [2] A. Pakou *et al.*, *Phys. Rev. Lett.* **90**, 202701 (2003).
- [3] A. R. Garcia, J. Lubian, I. Padron, P. R. S. Gomes, T. Lacerda, V. N. Garcia, A. Gómez Camacho, and E. F. Aguilera, *Phys. Rev. C* **76**, 067603 (2007).
- [4] Mandira Sinha *et al.*, *Phys. Rev. C* **76**, 027603 (2007).
- [5] C. Beck, N. Keeley, and A. Diaz-Torres, *Phys. Rev. C* **75**, 054605 (2007).
- [6] M. Biswas, S. Roy, M. Sinha, M. K. Pradhan, A. Mukherjee, P. Basu, H. Majumdar, K. Ramachandran, and A. Shrivastava, *Nucl. Phys.* **A802**, 67 (2008).
- [7] N. Keeley, K. W. Kemper, O. Momotyuk, and K. Rusek, *Phys. Rev. C* **77**, 057601 (2008).
- [8] S. Mukherjee, B. K. Nayak, D. S. Monteiro, J. Lubian, P. R. S. Gomes, S. Appannababu, and R. K. Choudhury, *Phys. Rev. C* **80**, 014607 (2009).
- [9] M. Y. M. Hassan, M. Y. H. Farag, E. H. Esmael, and H. M. Maridi, *Phys. Rev. C* **79**, 064608 (2009).
- [10] Y. Kucuk, I. Boztosun, and N. Keeley, *Phys. Rev. C* **79**, 067601 (2009).
- [11] D. S. Monteiro *et al.*, *Phys. Rev. C* **79**, 014601 (2009).
- [12] J. Lubian, T. Correa, E. F. Aguilera, L. F. Canto, A. Gomez-Camacho, E. M. Quiroz, and P. R. S. Gomes, *Phys. Rev. C* **79**, 064605 (2009).
- [13] P. R. S. Gomes *et al.*, *Nucl. Phys.* **A828**, 233 (2009).
- [14] L. F. Canto, P. R. S. Gomes, J. Lubian, L. C. Chamon, and E. Crema, *Nucl. Phys.* **A821**, 51 (2009).
- [15] V. N. Garcia, J. Lubian, P. R. S. Gomes, A. Gomez-Camacho, and L. F. Canto, *Phys. Rev. C* **80**, 037602 (2009).
- [16] F. A. Souza *et al.*, *Nucl. Phys.* **A821**, 36 (2009).
- [17] J. M. Figueira *et al.*, *Phys. Rev. C* **73**, 054603 (2006).
- [18] F. A. Souza, L. A. S. Leal, N. Carlin, M. G. Munhoz, R. Liguori Neto, M. M. de Moura, A. A. P. Suaide, E. M. Szanto, A. Szanto de Toledo, and J. Takahashi, *Phys. Rev. C* **75**, 044601 (2007).
- [19] A. Gómez Camacho, P. R. S. Gomes, J. Lubian, and I. Padrón, *Phys. Rev. C* **77**, 054606 (2008).
- [20] J. J. Kolata *et al.*, *Phys. Rev. C* **75**, 031302(R) (2007).
- [21] A. C. Shotter, A. N. Bice, J. M. Wouters, W. D. Rae, and J. Cerny, *Phys. Rev. Lett.* **46**, 12 (1981).
- [22] J. Hesselbarth and K. T. Knöpfle, *Phys. Rev. Lett.* **67**, 2773 (1991).
- [23] V. Guimarães *et al.*, *Phys. Rev. Lett.* **84**, 1862 (2000).
- [24] J. J. Kolata *et al.*, *Phys. Rev. C* **63**, 024616 (2001).
- [25] C. Signorini *et al.*, *Phys. Rev. C* **67**, 044607 (2003).
- [26] A. Shrivastava, A. Navin, N. Keeley, K. Mahata, K. Ramachandran, V. Nanal, V. V. Parkar, A. Chatterjee, and S. Kailas, *Phys. Lett.* **B633**, 463 (2006).
- [27] A. Pakou *et al.*, *Phys. Lett.* **B633**, 691 (2006).
- [28] A. Pakou *et al.*, *Phys. Rev. C* **76**, 054601 (2007).
- [29] D. Martínez Heimann *et al.*, *AIP Conf. Proc.* **1098**, 275 (2009).
- [30] S. Santra, V. V. Parkar, K. Ramachandran, U. K. Pal, A. Shrivastava, B. J. Roy, B. K. Nayak, A. Chatterjee, R. K. Choudhury, and S. Kailas, *Phys. Lett.* **B677**, 139 (2009).
- [31] G. Passatore, *Nucl. Phys.* **A95**, 694 (1967).
- [32] M. A. Nagarajan, C. C. Mahaux, and G. R. Satchler, *Phys. Rev. Lett.* **54**, 1136 (1985).
- [33] G. R. Satchler, *Phys. Rep.* **199**, 147 (1991).
- [34] C. Mahaux, H. Ngô, and G. R. Satchler, *Nucl. Phys.* **A449**, 354 (1986).
- [35] J. S. Toll, *Phys. Rev.* **104**, 1760 (1956).
- [36] W. Schutzer and J. Tiomno, *Phys. Rev.* **83**, 249 (1951).
- [37] L. F. Canto, P. R. S. Gomes, R. Donangelo, and M. S. Hussein, *Phys. Rep.* **424**, 1 (2006).
- [38] P. R. S. Gomes *et al.*, *Phys. Rev. C* **71**, 034608 (2005).
- [39] M. S. Hussein, P. R. S. Gomes, J. Lubian, and L. C. Chamon, *Phys. Rev. C* **73**, 044610 (2006).
- [40] J. M. Figueira *et al.*, *Phys. Rev. C* **75**, 017602 (2007).
- [41] H. Kumawat *et al.*, *Phys. Rev. C* **78**, 044617 (2008).
- [42] N. Keeley, S. J. Bennett, N. M. Clarke, B. R. Fulton, G. Tungate, P. V. Drumm, M. A. Nagarajan, and J. S. Lilley, *Nucl. Phys.* **A571**, 326 (1994).
- [43] A. M. M. Maciel *et al.*, *Phys. Rev. C* **59**, 2103 (1999).
- [44] C. Signorini *et al.*, *Phys. Rev. C* **61**, 061603(R) (2000).
- [45] S. B. Moraes, P. R. S. Gomes, J. Lubian, J. J. S. Alves, R. M. Anjos, M. M. Sant'Anna, I. Padrón, C. Muri, R. Liguori Neto, and N. Added, *Phys. Rev. C* **61**, 064608 (2000).
- [46] J. Lubian, I. Padron, P. R. S. Gomes, A. M. M. Maciel, R. M. Anjos, S. B. Moraes, J. J. S. Alves, C. Muri, R. Liguori Neto, and N. Added, *Phys. Rev. C* **64**, 027601 (2001).
- [47] A. Pakou *et al.*, *Phys. Lett.* **B556**, 21 (2003).
- [48] A. Pakou *et al.*, *Phys. Rev. C* **69**, 054602 (2004).
- [49] R. J. Woolliscroft, B. R. Fulton, R. L. Cowin, M. Dasgupta, D. J. Hinde, C. R. Morton, and A. C. Berriman, *Phys. Rev. C* **69**, 044612 (2004).
- [50] P. R. S. Gomes *et al.*, *Phys. Rev. C* **70**, 054605 (2004).
- [51] P. R. S. Gomes *et al.*, *J. Phys. G: Nucl. Part. Phys.* **31**, S1669 (2005).
- [52] P. R. S. Gomes *et al.*, *Phys. Rev. C* **73**, 064606 (2006).
- [53] J. Lubian *et al.*, *Nucl. Phys.* **A791**, 24 (2007).
- [54] A. Gómez Camacho, P. R. S. Gomes, J. Lubian, E. F. Aguilera, and I. Padrón, *Phys. Rev. C* **76**, 044609 (2007).
- [55] A. Pakou, *Phys. Rev. C* **78**, 067601 (2008).
- [56] E. F. Aguilera *et al.*, *Phys. Rev. C* **79**, 021601(R) (2009).
- [57] J. Wilczynski and K. Siwek-Wilczynska, *Phys. Lett.* **B55**, 270 (1975).
- [58] M. H. Macfarlane and S. C. Pieper, Argonne National Laboratory Report ANL-76-11, Rev. 1, 1978 (unpublished).
- [59] M. Rhoades-Brown, M. H. Macfarlane, and S. C. Pieper, *Phys. Rev. C* **21**, 2417 (1980).
- [60] M. E. Brandan, J. R. Alfaro, A. Menchaca-Rocha, J. Gómez del Campo, G. R. Satchler, P. H. Stelson, H. J. Kim, and D. Shapira, *Phys. Rev. C* **48**, 1147 (1993).
- [61] D. Abriola *et al.*, *Phys. Rev. C* **39**, 546 (1989).
- [62] D. Abriola *et al.*, *Phys. Rev. C* **46**, 244 (1992).
- [63] C. Muri *et al.*, *Eur. Phys. J. A* **1**, 143 (1998).
- [64] B. R. Fulton, D. W. Banes, J. S. Lilley, M. A. Nagarajan, and I. J. Thompson, *Phys. Lett.* **B162**, 55 (1985).
- [65] J. S. Lilley, M. A. Nagarajan, D. W. Banes, B. R. Fulton, and I. J. Thompson, *Nucl. Phys.* **A463**, 710 (1987).